

The structure of contact binaries

H. Kähler

Hamburger Sternwarte, Gojenbergsweg 112, D-21029 Hamburg, Germany (e-mail: hkaehler@hs.uni-hamburg.de)

Received / Accepted

Abstract. In radiative layers of rotating stars the luminosity carried by circulation currents through a surface of constant entropy (circulation luminosity) is shown to be positive. The corresponding decrease in the temperature gradient is important in the secondary of contact binaries. This result removes the deadlock in the theory of contact binaries.

The resulting treatment of contact binaries is investigated, assuming thermal equilibrium. The sources of the circulation luminosity in the secondary can be written as the product of a circulation function (a normalized non-negative function of the fractional mass) and an amplitude. If the amplitude is adjusted to give a prescribed temperature difference $\Delta T_e = T_{e1} - T_{e2}$, the choice of the circulation function is (in a broad range) unimportant. This invariance extends in a close approximation to all observable properties as well as to the internal structure. The temperature difference is bound to be positive. The fractional extent of radiative regions is larger in the secondary than in the primary. In the course of evolution the period increases and the mass ratio decreases. Comparing thermodynamic quantities on level surfaces, pressure and density are larger in the secondary than in the primary. The specific entropy is larger in the primary than in the secondary. The temperature difference is remarkably small and almost vanishing when averaged over the level surfaces occupied in both components.

The only free parameter (apart from ΔT_e) is the efficiency f_E of the energy transfer from the primary to the secondary. Using standard values for the parameters, a survey of unevolved and evolved contact configurations is presented. Observational tests are passed. In stable systems the degree of contact is small. Stable systems in the period-colour diagram, unevolved and evolved, cover the strip (and only the strip) of observed systems in this diagram. Lower limits for period and effective temperature, compatible with the observed limits, are caused by the requirement of thermal stability. Stable systems with mass ratios very close to unity are possible, in accordance with recent observations. Since stability considerations are essential in these observational tests the results support the assumption of thermal equilibrium as well as the treatment of the stability problem.

Models for individual observed systems with reliable data are well-determined (apart from some freedom in ΔT_e) and can be used to calibrate the efficiency and to determine metallicity and age. All models obtained so far are stable. This again supports the assumption of thermal stability. The results show that evolutionary effects are important and that the efficiency is very small ($f_E = 10^{-3} \dots 10^{-5}$).

Arguments are presented that the velocity field in the common envelope has a reversing layer, with motions from the secondary to the primary in the layers just above the critical surface and from the primary to the secondary in the surface layers.

Key words. stars: binaries: close – stars: rotation

1. Introduction

This paper is the third one in a systematic attempt to overcome the deadlock in the theoretical treatment of contact binaries. In the first paper (Kähler 2002, hereafter K1) we discussed the uncertainties in the structure equations. Serious uncertainties were found to concern only the energy sources and sinks associated with internal mass motions. In the second paper (Kähler 2002, hereafter K2) we made the usual assumption (hereafter assumption A) that sources and sinks occur only in the common envelope. Investigating a typical system we found a variety of solutions which are reasonable from an observational point of view, but all of them suffer from theoretical deficiencies. In particular, all solutions with good light curves (i.e. a small temperature difference between the components) are of the type proposed by Moss & Whelan (1973), i.e. the energy

sources in the secondary's envelope occur in the extreme superadiabatic layers. As shown by Hazlehurst (1974) this is impossible since the heat capacity of these layers is too small.

The results in K2 show that assumption A is too restrictive. When thermal equilibrium is assumed this conclusion is cogent since it does not depend on details, e.g. the choice of a transport equation for the energy transfer from the primary to the secondary. In the case of thermal cycles there is more freedom since they depend on the transport equation as well as on the equation governing the rate of mass exchange. Nevertheless the experience of decades shows that the conclusion is justified also in this case. Associated to a cycle is a configuration in unstable thermal equilibrium. If this configuration is in shallow contact (and if extreme superadiabatic transfer is excluded) the temperature difference is large for a considerable part of the

cycle. If the configuration is in good contact the temperature difference is always large. In both cases the light curve is bad.

Assumption A turns out to be a deadlock in the treatment of contact binaries. Energy sources or sinks in the interior of at least one component and corresponding changes in the temperature gradient are necessary. According to Lucy (1968) there is no freedom in the structure of radiative regions since the luminosity carried by circulation currents through a level surface vanishes (hereafter Lucy's theorem). The only remaining freedom concerns the extent of turbulent regions. A decrease of a convective envelope is in conflict with Lucy's theorem. An increase of the turbulent envelope in the secondary is in conflict with Roche geometry. An increase in the primary is compatible with Roche geometry, but the resulting model (Kähler 1989, Kähler & Fehlberg 1991) is in conflict with the second law of thermodynamics (Hazlehurst 1993) since (in a large region) internal mass motions transfer energy from cooler to hotter layers.

Accordingly, the deadlock boils down to Lucy's theorem. This theorem has been derived — also by Mestel (1965) and Roxburgh et al. (1965) — assuming that all thermodynamic quantities are constant on equipotential surfaces, i.e. assuming pseudo-barotropic layers in strict hydrostatic equilibrium. Although the theorem is usually taken for granted (e.g. Maeder & Zahn 1998), it is valid only in the zero-order approximation and not in higher approximations (Mestel 1965). In contact binaries departures from strict hydrostatic equilibrium (and thus baroclinic effects) are necessary for the energy transfer from the primary to the secondary, and baroclinic effects are expected to be important also in the interior of the components since the variation of the gravity on a level surface is large. For these reasons it is likely that Lucy's theorem does not apply. As observed also by Tassoul & Tassoul (1995) in a discussion of rotating stars there is no reason to claim that the net flux of energy carried by the circulation currents through each level surface vanishes.

Removing the deadlock and assuming thermal equilibrium we are able to predict the modification of the original Lucy (1968) model which solves the contact binary problem. Roche geometry requires that (in comparison with the Lucy model) either the (averaged) temperature gradient in the primary be increased or that the gradient in the secondary be decreased. An enhanced gradient is in conflict with the second law. Accordingly we need a reduced gradient in the secondary and thus a reduced radiative luminosity and/or a reduced extent of convective layers. The reduction is possible if some part of the luminosity in the secondary's interior is carried by circulation currents to the common envelope.

In this paper we investigate the resulting treatment of contact binaries, assuming that thermal equilibrium is enabled by circulation currents in the secondary's interior. We discuss the effects of circulation, present a survey of unevolved and evolved theoretical configurations, and perform observational tests. Having obtained models for individual observed systems we shall finally return to the hydrodynamic problem.

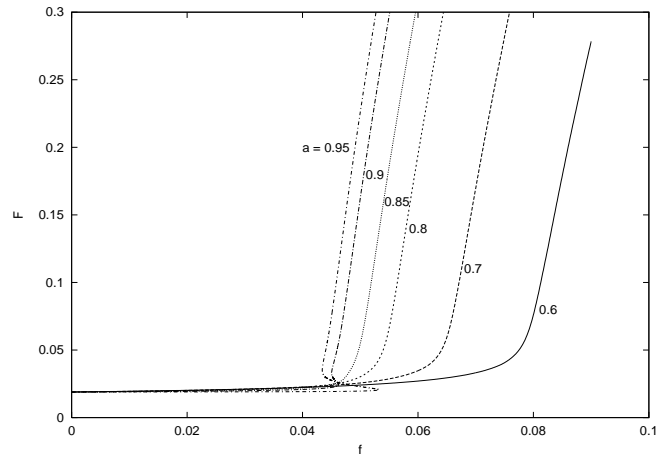


Fig. 1. The degree of contact F in dependence on the amplitude f of the circulation in System 1, for different values of the parameter a (see text).

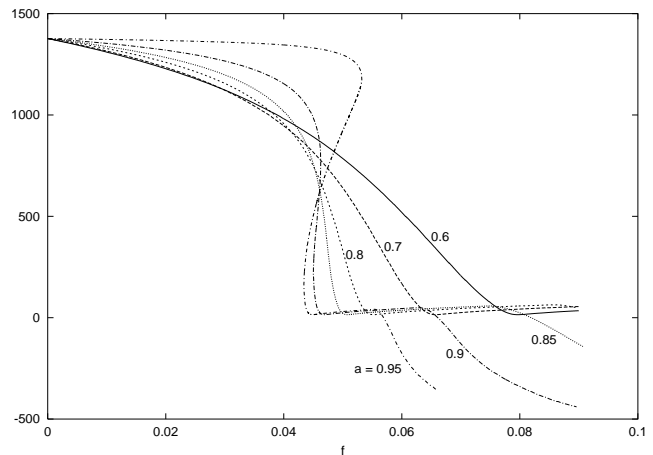


Fig. 2. The temperature difference ΔT_e in dependence on the amplitude f in System 1, for different values of the parameter a .

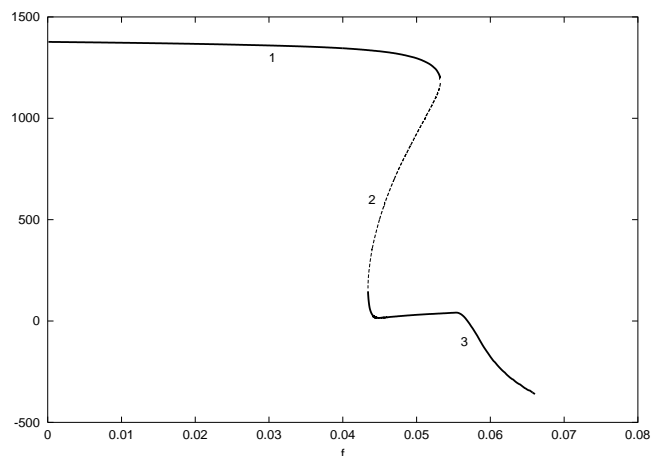


Fig. 3. ΔT_e as a function of f for $a = 0.95$ in System 1. Branches 1 and 3 (solid lines) of the linear series are stable, while branch 2 (dashed line) is unstable (see text).

2. The effects of circulation currents

We shall adhere to the notation of K1 and K2. Roche geometry is valid in a close approximation and will be assumed throughout this paper, apart from the discussion of the velocity field of the internal mass motions in Sect. 5.1. An equation for the transfer of mass between the components will not be needed. The energy transfer from the primary to the secondary will be treated as proposed in K1, assuming $\alpha_1 = \alpha_2$. Recall that α denotes the extent of the energy sinks/sources in the primary's/secondary's envelope, expressed as fractional mass of the layers above the critical surface. Since extreme superadiabatic transfer is not possible, the case of $\alpha \ll 1$ is excluded. Since the transfer occurs in the common envelope, values of α much larger than unity are also excluded. The parameter f_E , measuring the efficiency of the energy transfer, is certainly smaller than unity and possibly much smaller. The mixing length in units of the pressure scale height will taken to be $\alpha_+ = 1.5$. We shall assume that the extent of turbulent regions is determined by the Schwarzschild criterion ($i_t = 0$).

With these assumptions we have so far only two free parameters α , f_E . An additional parameter will be required when introducing circulation currents in the secondary. A modification of the structure equations derived in K1 will also be required.

2.1. Energy balance and temperature gradient

In the common envelope the luminosity Λ is transferred from the primary to the secondary (hereafter process 1). Let us assume that in addition in the secondary a fraction f of Λ is transferred by circulation currents from the interior to the envelope (process 2). Here we collect the equations describing the superposition of these processes.

The local balance of energy in the component i is

$$\partial l_i / \partial m_i = \varepsilon_i - T_i \dot{s}_i + \sigma_i, \quad (1)$$

where σ_i represents the sources or sinks in the envelope caused by process 1, i.e. by the energy transfer from the primary to the secondary in a region described by the parameter α . (Although thermal equilibrium is assumed, the time-dependent form of the energy balance is needed when discussing thermal stability.) Note that σ_2 does not allow for process 2.

In the presence of circulation in a radiative region of the secondary the luminosity is the sum

$$l_2 = l_{\text{rad},2} + l_{\text{circ},2} \quad (2)$$

of the radiative luminosity $l_{\text{rad},2}$ and the luminosity carried by circulation currents $l_{\text{circ},2}$ (hereafter circulation luminosity). The temperature gradient in a radiative layer

$$\nabla_{\text{rad},2} = \frac{3}{16\pi\alpha c G} \frac{\kappa_2 l_{\text{rad},2} P_2}{m_2 T_2^4} \quad (3)$$

is coupled with $l_{\text{rad},2}$ and not with l_2 . (Thus, in the presence of circulation Eq. (5) in K1 is not valid.) The borders of convective regions are therefore also coupled with $l_{\text{rad},2}$. Circulation occurs as well in convective regions (e.g. Kippenhahn 1963).

To investigate the effects of process 2 we shall assume a run of $l_{\text{circ},2}$ throughout the secondary as a non-negative function

of the mass variable which vanishes at the boundaries. (Since process 2 amounts to a redistribution of energy, the sources of the circulation luminosity, i.e. the regions with a positive derivative $dl_{\text{circ},2}/dm_2 > 0$, are compensated by sinks with a negative derivative.) Equations (2) and (3) define the radiative gradient $\nabla_{\text{rad},2}$. If this gradient is not larger than the adiabatic gradient the layer is radiative. Otherwise the layer is convective and the temperature gradient can be obtained from the mixing-length theory. Accordingly, the temperature gradient is determined as usual, replacing simply the luminosity l_2 by the radiative luminosity $l_{\text{rad},2}$. We have tacitly assumed that $l_{\text{rad},2}$ is positive apart from the centre. Otherwise the choice of $l_{\text{circ},2}$ is unphysical.

Writing the circulation luminosity as a function of the fractional mass $x_2 = m_2/M_2$, we shall assume that the derivative is a superposition

$$dl_{\text{circ},2}/dx_2 = f\Lambda c(x_2) + \dots \quad (4)$$

of sources and sinks. In the first term, representing the sources, $c(x_2)$ is a normalized non-negative function which will be called circulation function. The amplitude f is expected to be small compared to unity in realistic models with typical mass ratios. The dots represent corresponding sinks in the envelope with a distribution described again by the parameter α .

2.2. The choice of the circulation function

Since so far nothing is known about realistic circulation functions, two simple functions depending on a parameter a will be used. Writing for simplicity x instead of x_2 , the first function

$$c_1 = \begin{cases} \{1 + \cos[\pi(x-a)/d]\} / (2d) & \text{if } x > a - d \\ 0 & \text{otherwise} \end{cases} \quad (5)$$

with $d = x_f - a$ (where x_f represents the fitting mass) has its maximum at $x = a$. The second function

$$c_2 = \begin{cases} 0 & \text{if } x \leq a \\ V \{1 - \cos[\pi(x-a)/(b-a)]\} & \text{if } a < x < b \\ 2V & \text{if } x \geq b \end{cases} \quad (6)$$

with

$$b = (a + x_f)/2, \quad V = 1/(2x_f - a - b) \quad (7)$$

has a non-negative derivative, vanishes at the centre, and increases between $x = a$ and $x = b$.

As in K2 we investigate an unevolved system with the physical parameters

$$M = 1.6M_\odot, \quad J_{52} = 0.4, \quad X = 0.7, \quad Z = 0.02, \quad (8)$$

where J_{52} denotes the angular momentum in 10^{52} cgs-units (hereafter system 1). Using the parameters $\alpha = 0.5$, $f_E = 0.1$ and the circulation functions $c_1(a, x)$ with different values for a we calculated a continuous sequence of configurations in dependence on the amplitude f of the circulation, i.e. a linear series with the parameter f . Results for the temperature difference $\Delta T_e = T_{e1} - T_{e2}$ and the degree of contact F are shown in Figs. 1 and 2. In the absence of circulation ($f = 0$) the temperature difference is very large and the contact is shallow. We need

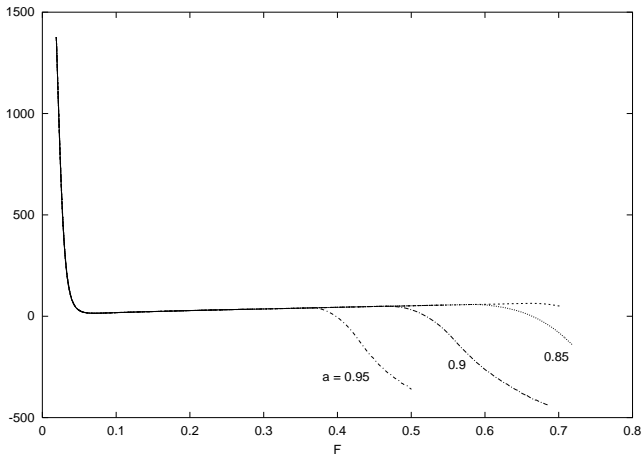


Fig. 4. The temperature difference ΔT_e as a function of F in System 1, for the same values of the parameter a as in Figs. 1 and 2.

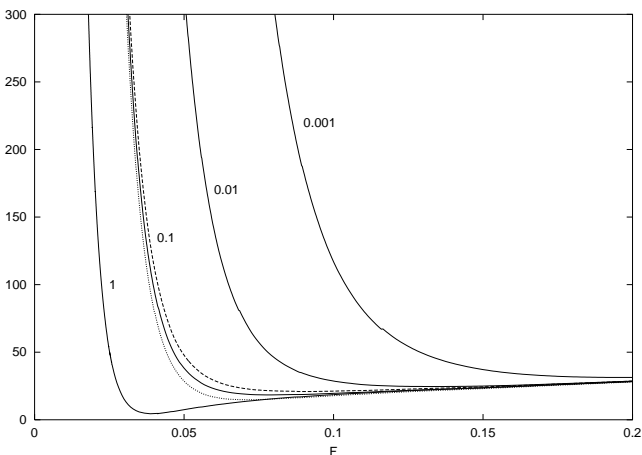


Fig. 5. ΔT_e as a function of F in System 1, for $\alpha = 1$ and different values of f_E (solid lines), for $\alpha = 0.5$, $f_E = 0.1$ (dotted line), and for $\alpha = 5$, $f_E = 0.1$ (dashed line).

configurations in shallow contact with a small temperature difference. For any choice of a they can be obtained with a small amplitude ($f \simeq 0.04 \dots 0.08$). This is as expected from the arguments collected in Sect. 1. Unfortunately the curves depend sensitively on a , i.e. on the choice of the circulation function which so far is unknown.

In particular, note that the linear series has turning points if a is sufficiently large ($a \geq 0.9$), i.e. if sources of the circulation luminosity occur only in outer layers. For $a = 0.95$ this is illustrated in Fig. 3. The curve consists of three branches. Configurations on branch 2 (dashed line) are unstable. Configurations which are reasonable from an observational viewpoint (in the neighbourhood of the turning point between branches 2 and 3) are either unstable or close to instability. Unstable configurations are unrealistic. Solutions which are stable but close to instability are extremely fragile from a computational viewpoint and thus probably also unrealistic. This suggests that the sources of the circulation luminosity occur not only in outer layers but also deep in the secondary's interior.

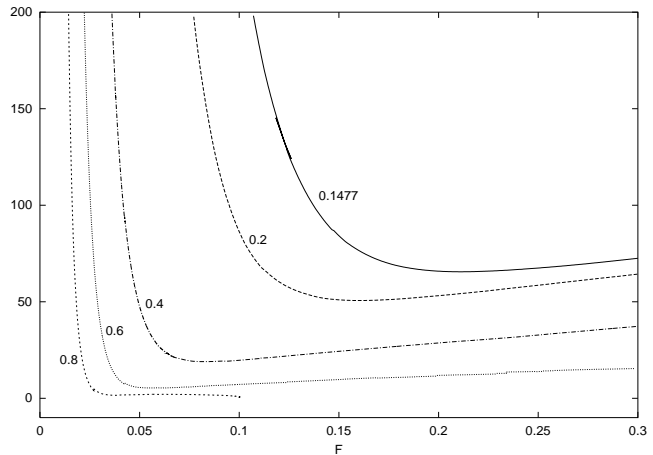


Fig. 6. Lines of constant angular momentum in the $(\Delta T_e, F)$ diagram for systems with $M = 1.6 M_\odot$. The numbers denote the mass ratio for $\Delta T_e = 200$ K (see text).

The uncertainty in the choice of the circulation function seems to be a serious drawback. However, if f is eliminated and ΔT_e considered as a function of F , all curves coincide apart from very large values for F which are not of interest. This surprising result is shown in Fig. 4. In other words, the relation between the two observable quantities ΔT_e and F does not depend on the choice of the circulation function. This invariance (which has been checked in numerous cases and which extends much further as we shall see) enables a treatment of contact binaries although so far we are not able to determine details of the circulation.

Figure 5 shows the relation between ΔT_e and F for system 1 in the region of interest (a small temperature difference and shallow contact) in more detail and for different values of the parameters α and f_E . The dependence on α is weak and can be neglected in an approximate treatment, but the dependence on f_E is important. The curve for $f_E = 1$ represents an unrealistic limiting case. Realistic values for f_E are certainly smaller than unity and probably much smaller. The curves show therefore that the temperature difference in system 1 is positive.

2.3. The temperature difference

Having seen that the temperature difference in system 1 is bound to be positive, here we ask whether this result can be generalized. As an example we consider unevolved systems of the same mass and composition as before, with $\alpha = 1$, $f_E = 0.1$. Figure 6 shows the invariant relation between ΔT_e and F in systems with different angular momentum. The curves are labeled by the mass ratio for $\Delta T_e = 200$ K. The curve beginning with $\Delta T_e = 200$ K and $q = 0.8$ ends up with $\Delta T_e \rightarrow 0$ and $q \rightarrow 1$, i.e. with a system with equal components.

It is manifest that the temperature difference is positive apart from the limiting case $q \rightarrow 1$. This result has been checked in many other cases. It is valid for all stable systems, evolved or unevolved.

Concerning a physically plausible interpretation, circulation currents tend to decrease the departures from hydrostatic equi-

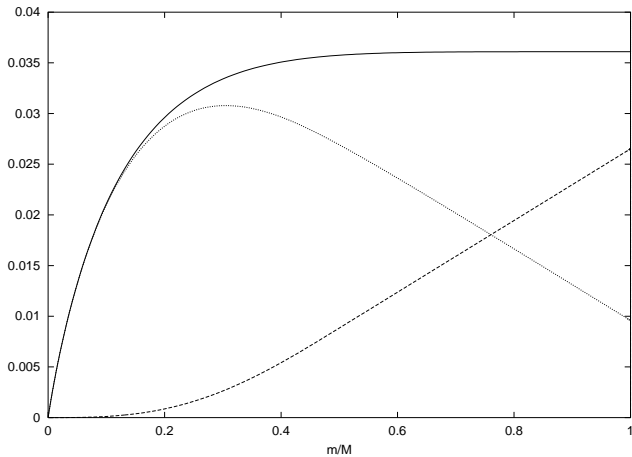


Fig. 7. Luminosities (in solar units) in the secondary's interior in System 2 in dependence on the fractional mass. The standard circulation function is used. The total luminosity (solid line) is the sum of the radiative luminosity (dotted line) and the circulation luminosity (dashed line).

librium in the whole system. Therefore they tend to reduce the temperature difference, which means that

$$d\Delta T_e/df < 0, \quad (9)$$

as it is the case in the relevant parts of the curves in Fig. 2 unless the branch is unstable, i.e. unless the parameter a is too large. Since the circulation currents do not quite succeed in removing the temperature difference, this difference remains positive.

In the example just considered the system with equal components is unstable, but systems with mass ratios up to $q = 0.9918$ are stable. For a very long time the absence of systems with nearly equal components seemed to be an established observational fact, and an instability of systems with $q \simeq 1$ was discussed as a possible theoretical explanation. The present example shows that the existence of systems with mass ratios very close to unity cannot be excluded from a theoretical viewpoint. This is in accordance with the observation of the system V 753 Mon with $q \simeq 0.97$ (Rucinski et al. 2000).

2.4. The treatment of contact binaries

The discussion in the preceding subsections has shown that in systems with typical mass ratios a small circulation luminosity (few percent of Λ) in the secondary's interior has a large influence on the structure. A similar circulation luminosity in the primary's interior has almost no effect since the radiative luminosity is much larger. For this reason circulation in the primary will be neglected, keeping in mind that in systems with large mass ratios the situation may be more complex.

To allow for circulation in the secondary we have to specify (i) a circulation function and (ii) the amplitude f or another measure for the strength of the circulation. Figure 2 shows that the amplitude which is necessary for a given temperature difference depends on the choice of the circulation function. To obtain a measure which is invariant the parameter f will be replaced by ΔT_e . In other words, the amplitude f will be ad-

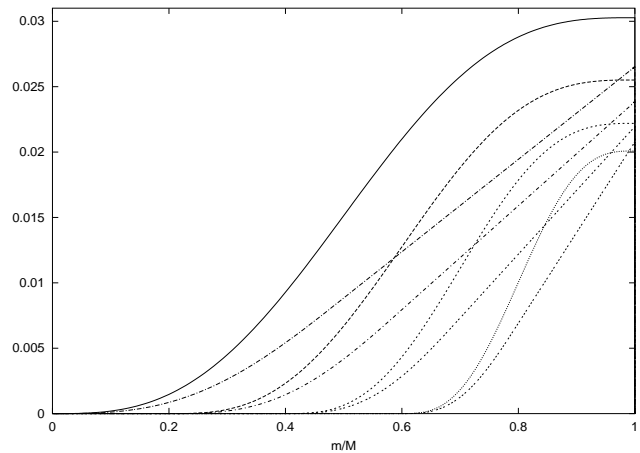


Fig. 8. The circulation luminosity in the interior of the secondary in System 2, in dependence on the fractional mass, for different circulation functions (see text).

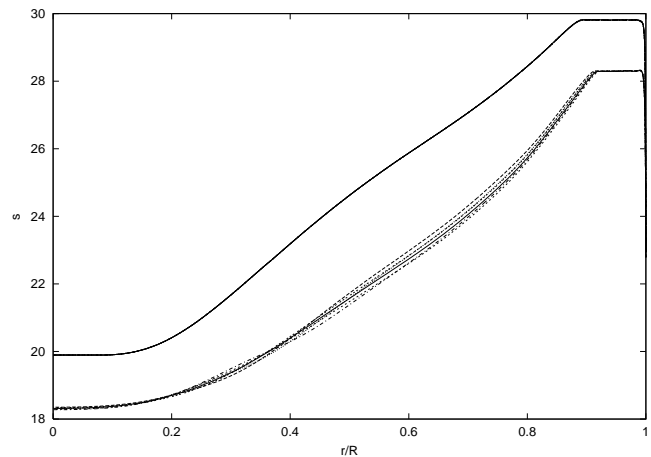


Fig. 9. The entropy distribution in System 2 in dependence on the fractional radius, for different circulation functions. The upper curves, representing the primary, coincide. The lower curves represent the secondary. Flat parts indicate convective regions.

justed to give the prescribed value for ΔT_e . The procedure is unique since in the case of a reasonable circulation function ($a < 0.85$ in the example considered) and a positive temperature difference the connection between amplitude and temperature difference is unique.

The resulting treatment of contact binaries is essentially based on the assumption of thermal stability. For given physical parameters (and mixing length) the structure of a configuration depends on the choice of the free parameters α , f_E , ΔT_e and on the choice of the circulation function. How large are the resulting uncertainties? We begin using the values

$$\alpha = 1, \quad f_E = 0.1, \quad \Delta T_e = 200\text{K}. \quad (10)$$

Keeping the parameters fixed, let us ask whether the observable properties depend on the choice of the circulation function. Results for system 1 are listed in Table 1. The first column contains the circulation function, the second one the parameter a .

Table 1. Observable properties of system 1 for $\alpha = 1$, $f_E = 0.1$, $\Delta T_e = 200$ K and different circulation functions (see text).

	a	P	q	T_e	L	L_1	L_2	R_1	R_2	F
c_1	0.5	0.2895	0.4195	5465	1.125	0.812	0.313	0.983	0.657	0.0341
c_1	0.6	0.2890	0.4196	5462	1.120	0.808	0.312	0.982	0.656	0.0342
c_1	0.7	0.2886	0.4195	5460	1.116	0.805	0.311	0.981	0.656	0.0342
c_1	0.8	0.2883	0.4196	5459	1.114	0.804	0.310	0.980	0.655	0.0343
c_2	0	0.2889	0.4194	5462	1.119	0.808	0.311	0.982	0.656	0.0342
c_2	0.1	0.2888	0.4193	5461	1.118	0.807	0.311	0.981	0.656	0.0343
c_2	0.2	0.2886	0.4193	5461	1.117	0.806	0.311	0.981	0.656	0.0343
c_2	0.3	0.2885	0.4192	5460	1.116	0.805	0.310	0.981	0.656	0.0343

Table 2. Observable properties of system 2 for $\alpha = 1$, $f_E = 0.1$, $\Delta T_e = 200$ K and different circulation functions.

	a	P	q	T_e	L	L_1	L_2	R_1	R_2	F
c_1	0.5	0.4182	0.3606	6368	4.024	2.994	1.030	1.397	0.873	0.0599
c_1	0.6	0.4179	0.3606	6367	4.018	2.989	1.029	1.396	0.873	0.0600
c_1	0.7	0.4177	0.3605	6366	4.014	2.987	1.028	1.396	0.872	0.0600
c_1	0.8	0.4176	0.3603	6366	4.012	2.985	1.027	1.396	0.872	0.0601
c_2	0	0.4177	0.3606	6367	4.017	2.989	1.029	1.396	0.872	0.0599
c_2	0.2	0.4177	0.3605	6367	4.015	2.987	1.028	1.396	0.872	0.0599
c_2	0.4	0.4175	0.3604	6367	4.013	2.985	1.027	1.395	0.872	0.0600
c_2	0.6	0.4175	0.3603	6366	4.012	2.985	1.026	1.395	0.872	0.0601

Table 3. Observable properties of system 1 in dependence on the free parameters.

α	f_E	ΔT_e	P	q	T_e	L	L_1	L_2	R_1	R_2	F
0.5	0.1	200	0.290	0.419	5461	1.122	0.810	0.312	0.984	0.657	0.033
1	0.1	200	0.289	0.419	5462	1.119	0.808	0.311	0.982	0.656	0.034
2	0.1	200	0.288	0.420	5463	1.118	0.806	0.311	0.980	0.656	0.035
1	0.0001	200	0.280	0.428	5435	1.086	0.776	0.309	0.971	0.660	0.141
1	0.001	200	0.284	0.419	5450	1.101	0.791	0.310	0.975	0.658	0.088
1	0.01	200	0.287	0.419	5458	1.111	0.800	0.311	0.978	0.656	0.055
1	0.1	200	0.289	0.420	5462	1.119	0.808	0.311	0.982	0.656	0.034
1	0.1	100	0.285	0.423	5469	1.106	0.779	0.327	0.972	0.653	0.040
1	0.1	200	0.289	0.419	5462	1.119	0.808	0.311	0.982	0.656	0.034
1	0.1	300	0.292	0.416	5455	1.131	0.835	0.296	0.990	0.659	0.031

Listed are the period P (in days), the mass ratio q , the mean effective temperature T_e , the total luminosity L (in solar units), the luminosities and radii of the components (in solar units), and the degree of contact F . Table 2 contains the corresponding results for the system with

$$M = 2M_{\odot}, J_{52} = 0.6, X = 0.7, Z = 0.02, \quad (11)$$

(hereafter system 2). Larger values for a than those included in the tables lead to configurations which are either close to instability or unstable. This shows again that the sources of the circulation extend deep into the secondary's interior.

Tables 1 and 2 show that the results for different circulation functions are in close agreement. The function c_1 with $a = 0.5$

represents a limiting case (a has the smallest possible value). If the results for this function (first line in the tables) is omitted, the agreement becomes excellent. We conclude that the choice of the circulation function (in a broad range) is unimportant as far as observable quantities are concerned. In other words, the invariance encountered in Sect. 2.2 extends in a close approximation to all observable properties. This invariance suggests the use of a standard circulation function. We decided to use the function c_2 with $a = 0$.

Consider next the effects of uncertainties in the free parameters. Results for system 1, obtained using the standard circulation function, are listed in Table 3, which is expected to cover the range of possible variations of the parameters. Changes in

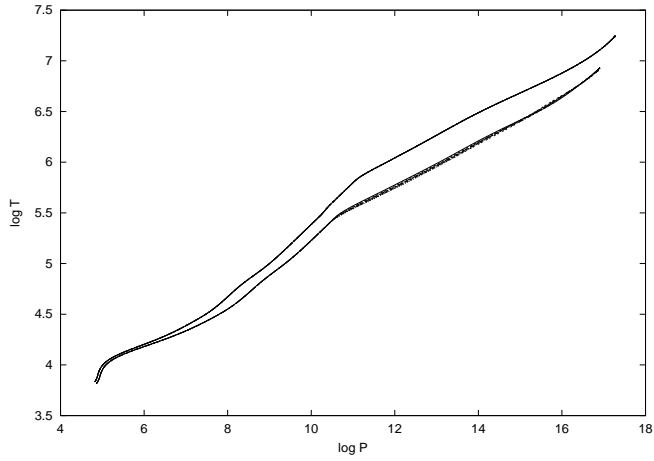


Fig. 10. The $\log P - \log T$ diagram in System 2, for different circulation functions. P is the pressure in cgs-units. The upper curves, representing the primary, coincide. The lower curves represent the secondary.

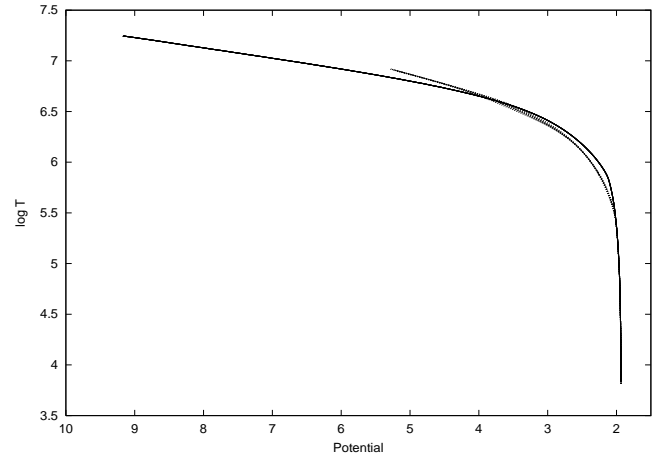


Fig. 12. $\log T$ as a function of the potential in System 2, for different circulation functions. The solid curves, representing the primary, coincide. The dotted curves represent the secondary.

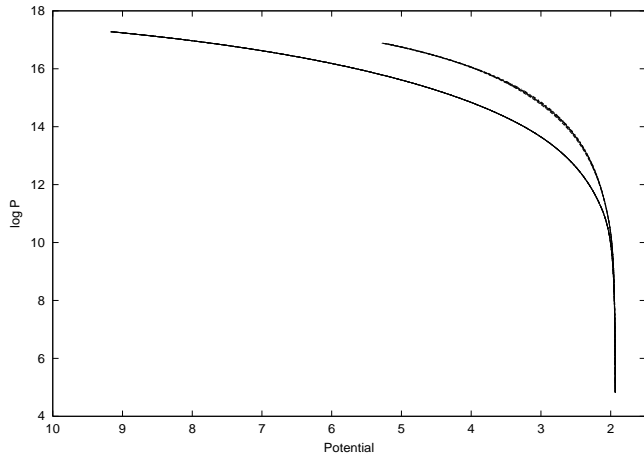


Fig. 11. $\log P$ as a function of the potential in System 2, for different circulation functions (see text). The lower curves, representing the primary, coincide. The upper curves represent the secondary.

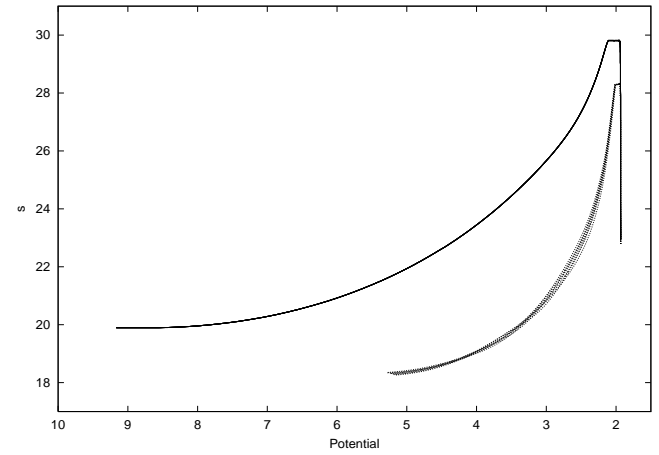


Fig. 13. The specific entropy s as a function of the potential in System 2, for different circulation functions. The solid curves, representing the primary, coincide. The dotted curves represent the secondary.

α have little influence, in accordance with a result from Fig. 5. An decrease in the efficiency f_E leads mainly to an increase in F (as it might have been expected) and to a decrease in the primary's luminosity. A change in the temperature difference affects all observable properties, particularly the light ratio.

Since these effects are only moderate, an approximate treatment of contact binaries is possible using standard values of the free parameters. When getting a first survey of contact configurations in Sect. 3 we shall use the values given in Eq. (10). In a next step observational tests can be used to improve these standard values. In particular, Table 3 shows that reliable observed values for F can be used to calibrate the efficiency. This will be done in Sect. 4.

2.5. The internal structure of the components

We shall first consider system 2 as a typical example for the internal structure of the components and for the influence of the choice of the circulation function. Figure 7 shows the luminosity in the secondary's interior as the sum of the radiative luminosity and the circulation luminosity. (The increase of the luminosity in the envelope escapes notice in this diagram.) The standard circulation function is used. Figure 8 shows the circulation luminosity in the secondary's interior for all circulation functions listed in Table 2. It is manifest that two classes of functions are used. The curve for the function c_1 with $a = 0.5$ (solid line) is untypical since the amplitude f is rather large. As mentioned already this function represents a limiting case which is unlikely to be realistic. In the further discussion this function will be omitted. In the following diagrams for system 2 the remaining seven circulation functions are used.

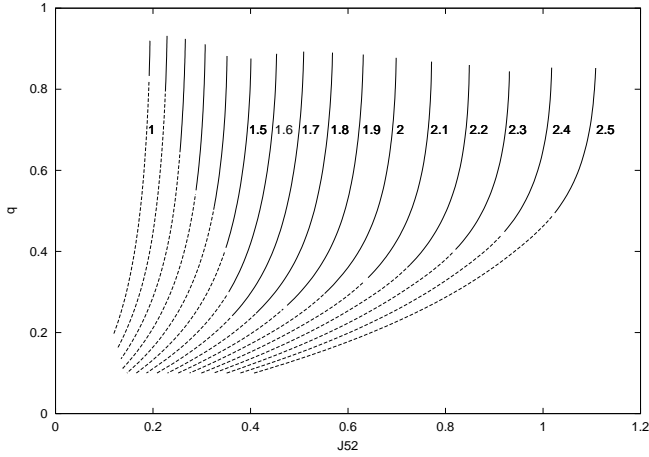


Fig. 14. The mass ratio q in dependence on the angular momentum J_{52} for unevolved systems with $Z = 0.02$ (see text). The numbers denote the mass in solar units. Solid/dashed lines represent systems of positive/negative charge.

Figure 9 shows the distribution of entropy (per nucleus divided by Boltzmann's constant). Flat parts of the curves indicate convective regions. The curves for the primary coincide. The curves for the secondary coincide only in the envelope. The uncertainty in deeper layers is not large. Note that the fractional extent in radius of the convective envelope is larger in the primary than in the secondary.

The $\log P - \log T$ diagram (Fig. 10) illustrates the close correlation of the two components in the outer layers. Again the curves for the primary coincide. The uncertainties in the secondary's curves are remarkably small.

Recall that in both components an effective central potential is well-defined, c.f. K1. Near the surface this potential coincides with the spherically averaged Roche potential. Recall furthermore that in the idealized case of strict hydrostatic equilibrium all thermodynamic quantities are constant on connected equipotential surfaces. Departures from strict equilibrium are necessary for the energy transfer. In particular, it is possible that circulation currents in the common envelope are driven by pressure differences on equipotential surfaces. Concerning the adjustment of circulation currents in the interior energy considerations might be important.

For these reasons it is of interest to investigate thermodynamic quantities in dependence of the potential. We shall use the normalized potential which is positive, somewhat smaller than 2 at the surface, and larger in the interior. Figure 11 shows $\log P$ as a function of the potential. The pressure difference $\Delta P = P_1 - P_2$ is negative throughout the system, including the outer layers. We found that this result is valid for any system, unevolved or evolved, for any mass and any mass ratio. Implications for the mass motions in the envelope will be discussed in Sect. 5.1.

Figure 12 shows $\log T$ in dependence on the potential. The temperature difference $\Delta T = T_1 - T_2$ is positive in the outermost layers, changes sign in deeper layers, and is always small. When averaged over all layers the difference is very small. This surprising result was again found to be valid for any system.

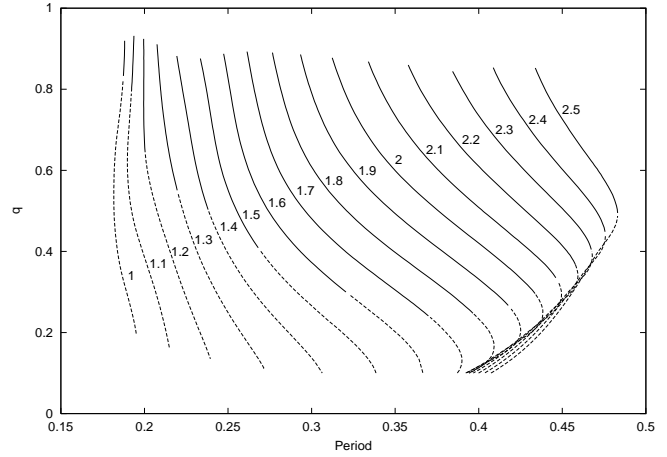


Fig. 15. The period-mass ratio diagram for unevolved systems with $Z = 0.02$. The symbols are as in Fig. 14.

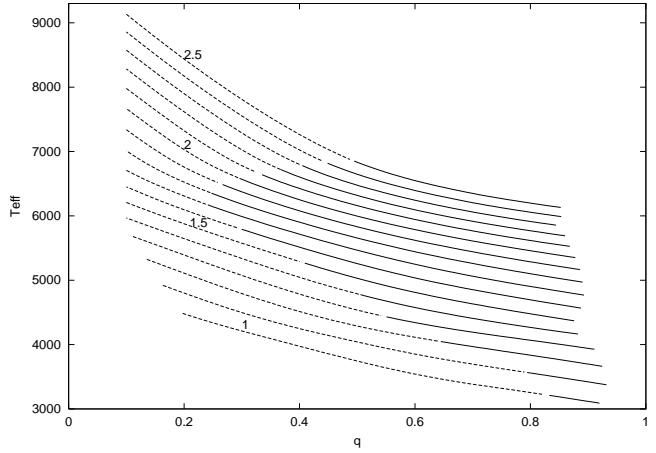


Fig. 16. The mean effective temperature in dependence on the mass ratio q for unevolved systems with $Z = 0.02$.

Combining the results for ΔP and ΔT and making use of the equation of state we conclude that the difference in density $\Delta \rho = \rho_1 - \rho_2$ is negative throughout the system. Consider finally the entropy difference $\Delta s = s_1 - s_2$ (Fig. 13). This difference is positive everywhere and large apart from the envelope.

From these results concerning differences of thermodynamic quantities on equipotential surfaces we see that most differences are large and have a characteristic sign. An exception is the difference in temperature which is small and almost vanishing when averaged over the level surfaces occupied in both components. The temperature is closely connected with the internal energy. A connection between the total energy of the system and the thermal adjustment suggests itself. We shall return to this point in a forthcoming paper.

This concludes the discussion of system 2. Results for system 1 are similar, with slightly larger uncertainties. Both systems have intermediate masses and mass ratios, and both systems are stable. When passing over to systems with smaller masses and/or smaller mass ratios, the uncertainties may increase and the stability may be lost. An example is the system

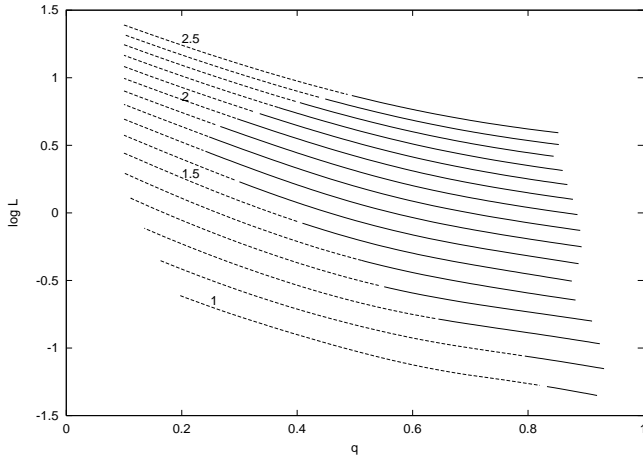


Fig. 17. $\log L$ (where L is the total luminosity in solar units) in dependence on the mass ratio q for unevolved systems with $Z = 0.02$.

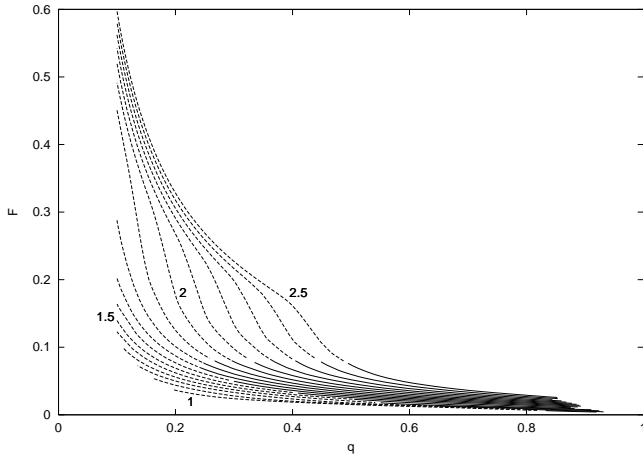


Fig. 18. The degree of contact F in dependence on the mass ratio q for unevolved systems with $Z = 0.02$.

with $M = 1M_{\odot}$ and $q = 0.32$. Since the secondary's mass is very small there is a strong tendency towards convection and thus little freedom for the effects of circulation in radiative regions. Entropy distribution and number and extent of convective regions depend strongly on the choice of the circulation function. Accordingly, the uncertainties in the internal structure are rather large in this case. These uncertainties do not extend to observable quantities. They are well defined. Uncertainties in the interior are not of interest since all configurations are unstable.

Summarizing, in stable systems the invariance found in the preceding subsections extends also to the internal structure of the components.

2.6. Remarks on the thermal stability problem

Recall first how the thermal stability of a configuration can be tested. A full test requires either a stability analysis (i.e. the inspection of eigenvalues) or evolutionary calculations, starting with small perturbations. A restricted test requires only the

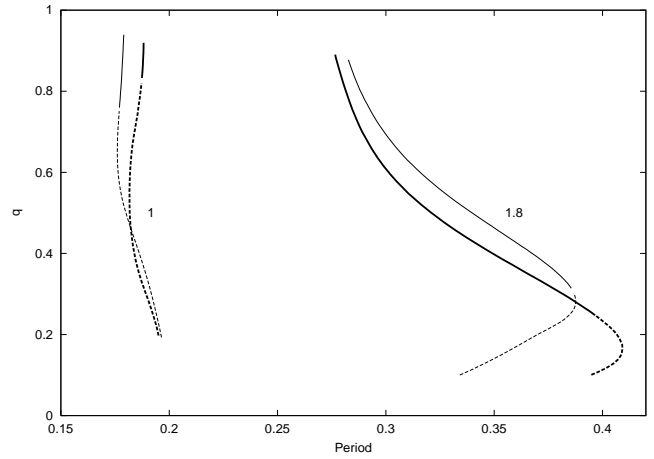


Fig. 19. Unevolved systems with $Z = 0.02$ (heavy lines) and $Z = 0.01$ (weak lines) in the period-mass ratio diagram. Solid/dashed lines indicate configurations of positive/negative charge. The numbers denote the mass in solar units.

charge c of a configuration, which is the sign of the Henyey determinant apart from a factor depending on the choice of the Henyey matrix. The charge $c = 1$ is necessary (but not sufficient) for stability, and the charge $c = -1$ indicates instability.

Consider the second test, i.e. the evolution following a small perturbation. The evolution can be calculated if the balance of energy and the temperature gradient are known at each point of time. In other words, we need the sources/sinks σ_i and the run of the circulation luminosity at each point of time.

The sources/sinks σ_i are approximately known if the transport equation for Λ is reasonable. Assuming that the transport equation here used [Eq. (49) in K1] is reasonable, this means that the choice of f_E is reasonable. The circulation luminosity is known if the circulation function (represented by the parameter a) and the amplitude f are known. Since there is a large freedom in the choice of the circulation function a can be kept fixed, but changes in f may be important.

Throughout this paper we assume that f is kept fixed during a perturbation. The resulting stability problem is well-defined but simplified. To make this point clear note that the present definition of the amplitude f is arbitrary and that other definitions are possible. For example, the expression $f\Lambda$ in the RHS of Eq. (4) could be replaced by fL or by fL_{\odot} or by some other expression. All these possibilities are equivalent as far as the structure of a configuration in thermal equilibrium is concerned since the amplitude is adjusted to the prescribed temperature difference. They are however *not* equivalent in the stability problem with a fixed amplitude. The resulting uncertainty in the stability problem remains to be investigated, but the results obtained so far suggest that the stability problem here used is reasonable.

All configurations of positive charge which have been tested so far turned out to be stable. For simplicity a configuration is therefore called stable if $c = 1$. If the stability has been tested by evolutionary calculations, this is mentioned.

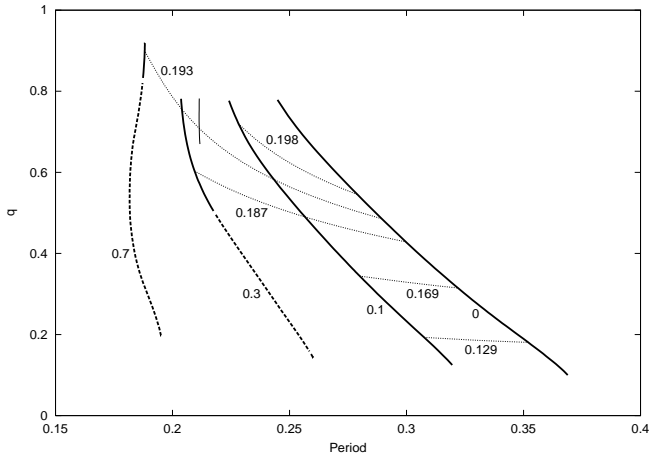


Fig. 20. Evolutionary effects in the period-mass ratio diagram for systems with $M = 1M_{\odot}$ and $Z = 0.02$ (see text). Shown are curves of constant hydrogen content in the primary's centre (heavy lines) and curves of constant angular momentum (dotted lines). The numbers denote X_{c1} and J_{52} , respectively. Solid and dashed lines are defined as in Fig. 19.

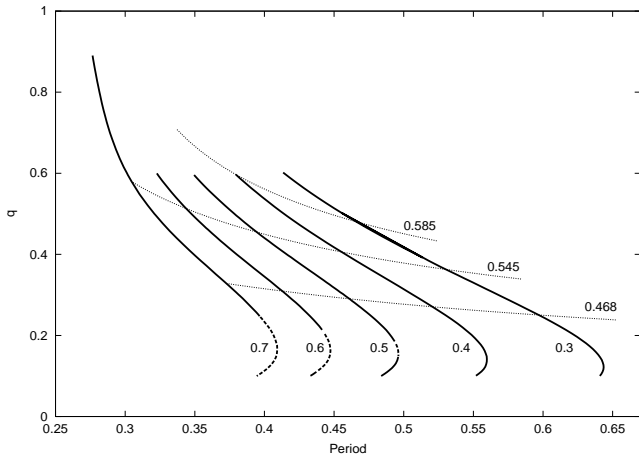


Fig. 21. Same as Fig. 20, but for systems with $M = 1.8M_{\odot}$.

3. A survey of contact configurations

In this section we present a survey of contact configurations, adopting the standard circulation function and the standard values (10) for the free parameters. Under these circumstances an unevolved configuration depends on three parameters (mass, angular momentum, metallicity). An evolved configuration depends in addition on the chemical profile in both components. In the simplest treatment of systems with intermediate or small mass ratios a simple chemical profile is assumed and evolutionary effects in the secondary are neglected. The evolutionary status is then described by the primary's central hydrogen content, and we are left with four parameters.

Since a complete survey is impossible we decided to discuss all unevolved configurations (in a certain mass range) with a standard composition, and to illustrate evolutionary effects and the effects of changes in metallicity in few examples. Further examples are given by the observed systems discussed

in Sect. 4. Examples for the effects of changes in the free parameters have already been discussed.

3.1. Unevolved configurations with $Z = 0.02$

We investigate systems with $X = 0.07$, $Z = 0.02$ in the mass range $1 \leq M/M_{\odot} \leq 2.5$. The lower mass limit is caused by the lack of opacities for low temperatures and large densities. [The opacities (OPAL 95 combined with opacities of Dave Alexander) have kindly been provided by A. Weiss.] For $M < 1.5M_{\odot}$ the opacities have been slightly extrapolated. For this reason and since complications in the equation of state (e.g. Coulomb interactions) are ignored, the treatment of systems with small masses is approximate only.

Figure 14 shows the mass ratio q as a function of the angular momentum J_{52} for different masses. The upper border of the region covered by configurations (near $q = 0.9$) is determined by the condition that the amplitude of the circulation is non-negative. In other words, the upper border is the curve $f = 0$ which is invariant. For smaller values of the temperature difference the upper border occurs at larger mass ratios.

The lower border is the line $q = 0.1$ since the Chebyshev approximation for the neck used in the numerical code (c.f. K1) is valid only for $q \geq 0.1$. An exception concerns small masses ($M \leq 1.3M_{\odot}$). For these masses the lower border, occurring at somewhat larger mass ratios, is caused by the prescribed temperature difference. Below the border the difference is bound to be larger than 200 K.

The relation between angular momentum and mass ratio for given mass is unique. Since the derivative dq/dJ_{52} is positive, the system with the largest mass ratio has the largest angular momentum. Systems of sufficiently large angular momentum (or mass ratio) are stable, while the remaining systems are unstable.

When passing over from intermediate to small masses the border between stable and unstable systems is shifting towards large mass ratios. For a mass somewhat smaller than the solar mass stability becomes impossible. This holds as well for smaller values of ΔT_e . Accordingly, there is a lower limit for the mass of unevolved contact binaries, and thus also a lower limit for the effective temperature. The limit is caused not by the lack of configurations but by their instability.

Figure 15 shows the period-mass ratio diagram. Solid lines represent again systems of positive charge. They do not cross, which implies that the structure of an unevolved system in thermal equilibrium with $Z = 0.02$ is (in a reasonable approximation) fully determined by two observable properties. In the mass range under consideration there is a minimum period of about 0.18 days which is compatible with the observed minimum of 0.221 days for CC Com. The maximum period (about 0.48 days) however is far below the observed maximum.

Figures 16–18 show characteristic properties in dependence on mass and mass ratio. The results for the degree of contact F offer an observational test. Observed values for F are usually small compared to unity. This is in accordance with the results in Fig. 18 since for all stable systems F is small compared to unity. This lends support for the treatment of the

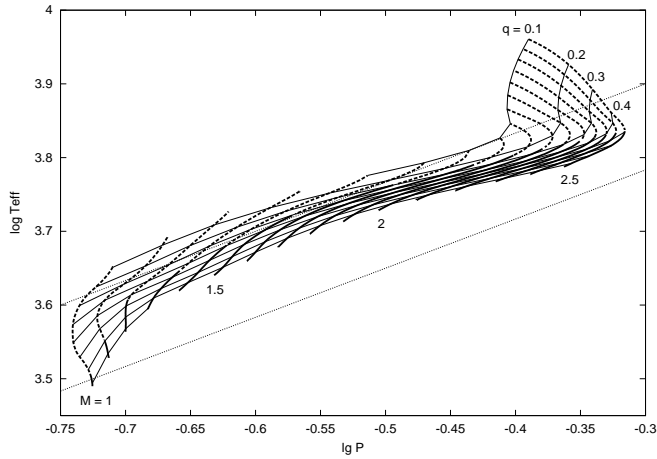


Fig. 22. The period-colour relation for unevolved systems with $Z = 0.02$. Shown are lines of constant mass (strong lines, solid/dashed for positive/negative charge) and of constant mass ratio (weak lines). Observed systems occur in the strip limited by the dotted lines.

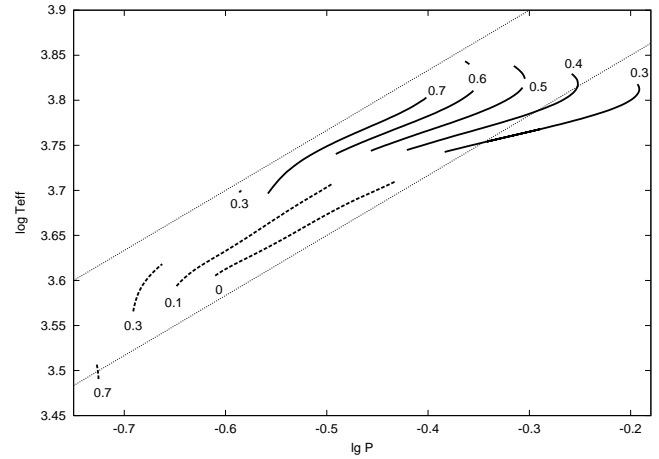


Fig. 24. The period-colour relation for stable evolved systems with $Z = 0.02$ and the masses $M = 1M_{\odot}$ (dashed lines) and $M = 1.8M_{\odot}$ (solid lines). The numbers denote the hydrogen content in the primary's centre.

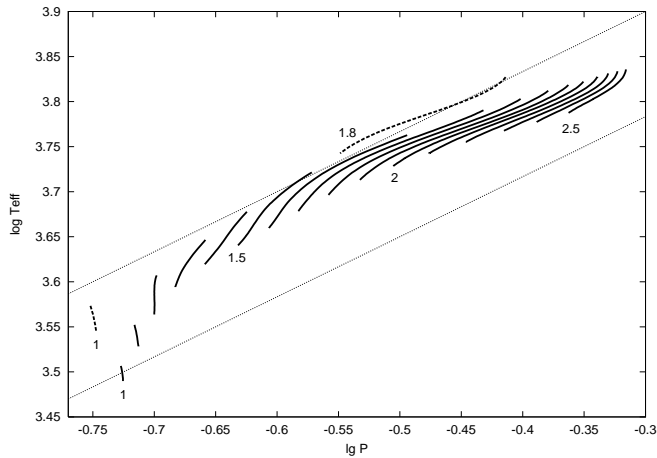


Fig. 23. The period-colour relation for stable unevolved systems with $Z = 0.02$ (solid lines) and $Z = 0.01$ (dashed lines). The numbers denote the mass in solar units.

stability problem. Recall that a rather large value for the efficiency ($f_E = 0.1$) is used. As shown in Table 3 a reduced efficiency leads to an enhanced (but still small) degree of contact.

3.2. Effects of metallicity changes

The results obtained so far do not cover the range of observed systems. This can best be seen in the period-mass ratio diagram (Fig. 15). Systems having large periods and intermediate or small mass ratios are absent. Stable systems with very small mass ratios are also absent. Since systems with these properties are observed, effects neglected so far have to be taken into account. Here we consider the effects of metallicity changes in unevolved systems.

The effects of a decrease in Z turned out to be small, apart from an increase in luminosity and effective temperature for

given mass and mass ratio. Figure 19 shows examples in the period-mass ratio diagram. Results for $M = 1M_{\odot}$ represent very small masses where the difficulties are largest. Results for $M = 1.8M_{\odot}$ represent typical masses. In both cases the influence of Z is weak only. In particular, apparently the lower limit for the period depends only slightly on Z . The absence of stable systems with large periods and intermediate or small mass ratios is even more pronounced when $Z = 0.01$. We conclude that metallicity effects cannot help to extend the range of stable systems in the period-mass ratio diagram.

3.3. Effects of evolution

Next we investigate evolutionary effects as the only remaining possibility to extend the range of stable systems. In the component i the simple hydrogen profile

$$X = \begin{cases} X_{ci} + (0.7 - X_{ci}) \sin[\pi x_i / (2x_c)] & \text{if } x_i \leq x_c \\ 0.7 & \text{otherwise} \end{cases} \quad (12)$$

will be assumed, depending on the central hydrogen content X_{ci} and a parameter x_c . The standard value $x_c = 0.5$ will be used. Effects of changes in x_c will be investigated when analysing individual observed systems in Sect 4.

In the general case both components are evolved and the evolutionary status is described by two parameters X_{c1}, X_{c2} . In an approximate treatment evolutionary effects in the secondary can be neglected unless the mass ratio is large, and the evolutionary status is described by one parameter X_{c1} .

Concerning the choice of the circulation function we checked the invariance and found that the use of the standard circulation function is justified also in evolved systems.

Evolutionary effects for systems with $M = 1M_{\odot}, Z = 0.02$ are shown in Fig. 20. Except for the thin solid line all curves have been calculated neglecting evolutionary effects in the secondary. Heavy lines represent configurations with a given value for X_{c1} . As before, solid/dashed lines represent configurations of positive/negative charge. Evolved configura-

tions with very large mass ratios ($q \gtrsim 0.8$) have been omitted. With decreasing X_{c1} the curves are shifting to the right, i.e. to larger periods, and the extent of stable configurations is increasing. Stable evolved systems with very small mass ratios exist for periods larger than about 0.3 days.

On the dotted curves the angular momentum is constant. Since in the course of evolution X_{c1} decreases and the angular momentum does not increase, the period increases and the mass ratio decreases. The lower limit for the period found in unevolved systems is therefore valid also for evolved systems.

In systems with large mass ratios the results are rough only since effects of nuclear evolution in the secondary are neglected. The influence of these effects can be seen if they are overestimated. This is the case in the thin solid line, which represents stable configurations with $X_{c1} = X_{c2} = 0.3$ and $q \lesssim 0.8$. The curves of constant angular momentum for $X_{c1} = X_{c2}$ almost coincide with the curves for $X_{c2} = 0.7$. Accordingly, the main results obtained neglecting evolutionary effects in the secondary (increase of period and decrease of mass ratio in the course of evolution) remain valid if these effects are taken into account.

A similar diagram for systems with $M = 1.8M_{\odot}$ is shown in Fig. 21. Again it can be seen that the evolution (with or without loss of angular momentum) proceeds towards larger periods and smaller mass ratios. Again stable evolved systems with very small mass ratios are found. Most important is the result that large periods and small mass ratios are possible among evolved systems.

We conclude that the structure of contact binaries depends sensitively on evolutionary effects and that the range of observed systems can be explained only by these effects.

3.4. The period-colour relation

The period-colour relation of observed contact binaries (Eggen 1961,1967) provides an important observational test. In the period-colour diagram (Figs. 22–24) the observed systems are mainly found in the strip limited by the dotted lines. Figure 22 shows stable and unstable unevolved configurations with $Z = 0.02$. Almost all configurations outside the strip are unstable.

Let the strip be divided in two strips of the same width (upper and lower strip, respectively). Figure 23 shows that stable unevolved systems cover roughly the upper strip, and Fig. 24 shows that stable evolved systems cover almost the full strip. Accordingly, the full strip is covered by stable systems, and stable systems outside the strip are almost absent.

These results lend support to the assumption of thermal equilibrium as well as to the treatment of the stability problem.

4. Individual observational tests

In this section individual observed systems with reliable data will be used as tests of the theory. First we shall ask whether such tests are severe and what we can learn from them.

Table 4. Models for AB And.

f_E	ΔT_e	Z	T_e	L	R_1	R_2	F
			5700	1.46	1.05	0.76	0.15
10^{-1}	200	0.010	5756	1.57	1.022	0.735	0.037
10^{-2}	200	0.010	5760	1.58	1.025	0.738	0.061
10^{-3}	200	0.010	5760	1.60	1.031	0.744	0.099
10^{-4}	200	0.010	5759	1.64	1.040	0.754	0.162
10^{-4}	200	0.011	5714	1.59	1.040	0.754	0.160
10^{-4}	100	0.011	5734	1.63	1.046	0.760	0.198

Table 5. Models for BV Dra.

f_E	ΔT_e	Z	T_e	L	R_1	R_2	F
			6190	2.29	1.12	0.76	0.114
10^{-1}	200	0.004	6333	2.49	1.091	0.723	0.050
10^{-1}	200	0.005	6251	2.36	1.091	0.723	0.048
10^{-1}	200	0.006	6172	2.24	1.091	0.723	0.047
10^{-1}	200	0.007	6095	2.13	1.090	0.723	0.046
10^{-2}	200	0.006	6175	2.27	1.095	0.728	0.079
10^{-3}	200	0.006	6174	2.30	1.102	0.735	0.129
10^{-3}	100	0.006	6192	2.35	1.106	0.739	0.158

Table 6. Models for BW Dra.

f_E	ΔT_e	Z	T_e	L	R_1	R_2	F
			5930	1.40	0.98	0.55	0.140
10^{-1}	200	0.006	5900	1.33	0.965	0.537	0.053
10^{-2}	200	0.006	5903	1.35	0.968	0.541	0.088
10^{-3}	200	0.006	5904	1.37	0.973	0.546	0.144
10^{-3}	200	0.005	5978	1.44	0.974	0.547	0.146
10^{-3}	100	0.005	5995	1.46	0.977	0.550	0.181

4.1. Observable quantities and degrees of freedom

We begin with an observational difficulty. A light curve synthesis requires an assumption concerning the distribution of surface brightness. Usually a gravity brightening law is assumed (sometimes with different exponents in the two components) and the temperature difference is treated as an adjustable parameter. (In particular, a negative temperature difference is adopted to reproduce the light curves of W-type systems.) The arbitrariness of this procedure is manifest. If a gravity brightening law exists there is no freedom in the temperature difference.

Actually there is no sound theoretical argument in favour of a correlation between local gravity and local effective temperature. In a rotating single star without complications (e.g. spots) an (individual) gravity brightening law exists already for symmetry reasons. In a contact binary symmetry arguments fail as well as physical arguments (c.f. Kähler & Fehlberg 1991), and a detailed mapping of the surface appears to be necessary as recognized already by Hilditch et al. (1988).

Table 7. Models for OO Aql.

f_E	Z	X_{c2}	X_{c1}	T_{e1}	L	R_1	R_2	F
				5700	3.30	1.39	1.29	0.27
10^{-2}	0.010	0.185	0.170	5939	3.54	1.318	1.218	0.061
10^{-2}	0.012	0.170	0.157	5836	3.30	1.318	1.218	0.060
10^{-3}	0.012	0.160	0.147	5827	3.33	1.328	1.228	0.097
10^{-4}	0.013	0.137	0.124	5758	3.26	1.345	1.245	0.159
10^{-5}	0.013	0.100	0.103	5736	3.36	1.375	1.275	0.264
10^{-5}	0.014	0.095	0.096	5685	3.24	1.373	1.274	0.259

In the present treatment the temperature difference is bound to be positive, and there is no freedom to explain the light curves of W-type systems with a negative difference. A negative difference is also in conflict with infrared observations (e.g. Hrivnak (1989) and UV observations (e.g. Ruciński 1993).

In view of these difficulties we consider the observed mean temperature as more reliable than the temperature difference, and the observed total luminosity L as more reliable than the luminosities L_1, L_2 of the components.

Period P , mass ratio q , mass M , mean temperature T_e , luminosity L , radii R_i , and degree of contact F will be taken as observational quantities. They are not independent. Recall that $R_i = \lambda_i A$, where the separation A of the components is a function of M and P on account of Kepler's law. The normalized radius λ_i is a function of q and F . The luminosity L is known if radii and temperature are known. We are left with $N_{\text{obs}} = 5$ independent observables P, q, M, T_e, F .

The degrees of freedom in a model are mass M , angular momentum (or period P), metallicity Z , central hydrogen content in the primary X_{c1} , and efficiency f_E . (There is little freedom in the temperature difference, and the effects of changes in α are unimportant). Accordingly, there are $N_{\text{free}} = 5$ degrees of freedom.

Since $N_{\text{free}} \geq N_{\text{obs}}$ there is freedom to fit a model to the observations. The tests involving individual systems are therefore not able to provide evidence for thermal equilibrium. Nevertheless they are important. Since $N_{\text{free}} = N_{\text{obs}}$ the model is well-determined. The structure of observed systems can therefore be determined, assuming thermal equilibrium, and the stability can be tested. In the case of instability either the treatment of the stability problem is insufficient or the system is in thermal imbalance. In the case of stability the efficiency can be calibrated.

4.2. The system AB And

For the system AB And ($P = 0.331892$ day) Hrivnak (1988) determined the mass ratio $q = 0.491$, the mass $M = 1.5M_{\odot}$, and other properties listed in the first line of Table 4, where temperatures are in Kelvin and luminosities and radii are in solar units. (This holds as well in the following tables.) The temperature is an average between the components. According to Hrivnak the uncertainty in L is large. Standard errors in the last digits are 1 for the radii and 3 for the degree of contact.

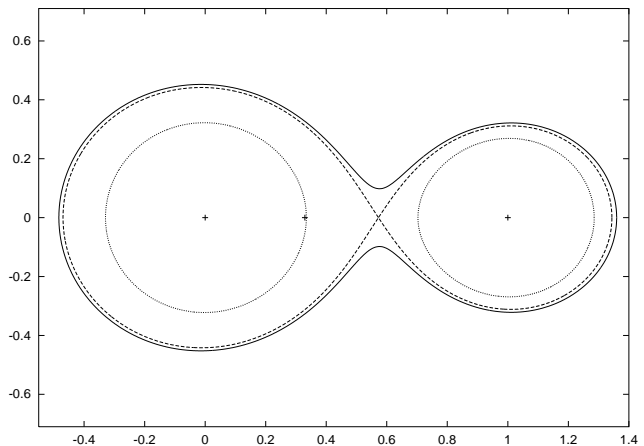


Fig. 25. The structure of AB And in the equatorial plane. Shown are the surface (solid line), the critical surface (dashed line), and the lower borders of the convective envelopes (dotted lines). The dots denote the centres of the components and the centre of mass.

Treating the observed values for period, mass, and mass ratio as constraints and using X_{c1} to adjust the mass ratio, a configuration is determined by the metallicity Z and the parameters $f_E, \Delta T_e$. Models for AB And are summarized in Table 4. The charge is positive and the models are indeed stable. This has been checked by evolutionary calculations following a small perturbations. The amplitude of the circulation is small ($f \simeq 0.04$). The models show that the theory is compatible with the observations. The results for the temperature suggests the metallicity $Z = 0.011$. The results for the degree of contact suggest a very small value for the efficiency ($f_E \simeq 10^{-4}$). The model with these two values and with $\Delta T_e = 200$ K is in excellent agreement with the observations, except for the radii which are somewhat too small. We shall return to this point.

The geometry of the system in the equatorial plane is shown in Fig. 25. Note that the fractional extent in radius of the convective envelope is much larger in the primary than in the secondary. The fractional extent in mass is also much larger.

We checked also the effects of changes in the chemical profile. In the models listed in Table 4, calculated with the standard profile ($x_c = 0.5$), the hydrogen content X_{c1} is somewhat lower than 0.4. Models with $x_c = 0.3$ give similar results with $X_{c1} \simeq 0.2$. Accordingly, the choice of the chemical profile is of

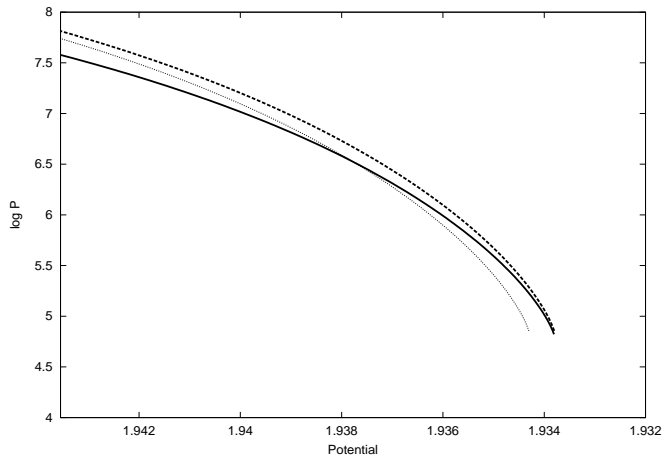


Fig. 26. $\log P$ as a function of the potential in the common envelope of system 2. The strong solid/dashed line represents the primary/secondary. The dotted line represents a modified run of pressure in the secondary (see text).

minor importance. The amount of hydrogen already converted to helium is also similar and can be used to estimate the age of the system.

4.3. The system BV Dra

The contact binaries BV Dra and BW Dra are particularly interesting since they form a visual binary. Precise observational results have been obtained by Kaluzny & Rucinski (1986). We begin with BV Dra. Period (0.350067 day), mass ($1.47M_{\odot}$) and mass ratio ($q = 0.411$) are again treated as constraints. Other observational results are listed in the first line of Table 5. Standard errors in the last digits are 21 for the luminosity, 1 for the radii, and 27 for the degree of contact.

The models of BV turned again out to be stable. Comparing the temperatures with the observed value we obtain the metallicity $Z = 0.006$, in accordance with the result of Kaluzny & Rucinski. The degree of contact suggests again a very low efficiency ($f_E \simeq 10^{-3}$). The model with these values and with $\Delta T_e = 200$ K is in very good agreement with the observations, again apart from the fact that the radii are somewhat too small.

4.4. The system BW Dra

The constraints for this system are $P = 0.292167$ day, $M = 1.18M_{\odot}$, $q = 0.280$. Other observational results are listed in the first line of Table 6. Standard errors in the last digits are 1 for the radii, 15 for the luminosity, and 34 for the degree of contact. Since no mean temperature has been reported by Kaluzny & Rucinski, a temperature somewhat smaller than the primary's polar temperature (5980 K) has been adopted, as it is the case in BV Dra.

The models are again stable. This has been checked in evolutionary calculations. The temperature suggests a metallicity $Z = 0.005 \dots 0.006$ which is very similar to the metallicity of BV Dra. This is as expected. The degree of contact suggests again the efficiency $f_E \simeq 10^{-3}$. Adopting these values and a

temperature difference $\Delta T_e = 200$ K, the agreement between theory and observations is very close.

4.5. The system OO Aql

The system OO Aql, observed by Hrivnak (1989), has a very large mass ratio ($q = 0.843$). Other constraints are $M = 1.92M_{\odot}$, $P = 0.506789$ day. The observed temperature difference $\Delta T_e = 65$ K has been added as a constraint. Other observed properties are listed in the first line of Table 7.

Since q is large, evolutionary effects in the secondary are important. (If they are ignored, the constraints require a negative amplitude f .) Table 7 contains properties of configurations for different combinations of X_{c1} and X_{c2} . These combinations are approximately determined by the condition that f is positive and small. Note that X_{c2} is only slightly larger than X_{c1} and that these values depend on the choice of x_c . Evolutionary effects are large in this system, in accordance with the result of Hrivnak. The configurations in the last two lines are in excellent agreement with the observations. The radii are slightly smaller than those given by Hrivnak. The agreement is nevertheless perfect. Hrivnak's radii are volume radii (c.f. Mochnacki 1984) and thus larger (in the present case by about 1.4 percent) than the radii in a spherically averaged treatment of the components (c.f. Kähler 1986). (A similar difference in radii occurs in the systems discussed above). The metallicity ($Z = 0.013 \dots 0.014$) turns out to be larger than estimated by Hrivnak. The efficiency is extremely small ($f_E \simeq 10^{-5}$), and the amplitude is rather large ($f \simeq 0.09$).

Again the stability was tested in evolutionary calculations. The two best models (in the last two lines of Table 7) are stable, but the other models are unstable. Apparently an extremely low efficiency (or a rather large degree of contact) is necessary for stability. This is suggested also by other models not listed in Table 7.

4.6. Conclusions

Several observed systems with well-determined parameters have been used as tests of the theory. In all cases an excellent agreement between theory and observations is obtained. This is as expected from the number of free parameters. In all systems evolutionary effects are important.

All systems turned out to be stable. This lends support not only to the transport equation used in the present model but also to the assumption of thermal equilibrium and to the treatment of the stability problem.

The efficiency was determined to be very small ($f_E \simeq 10^{-3} \dots 10^{-5}$). This shows that the velocities of the internal mass motions in the neighbourhood of the inner Lagrangian point are much smaller than the sound velocity.

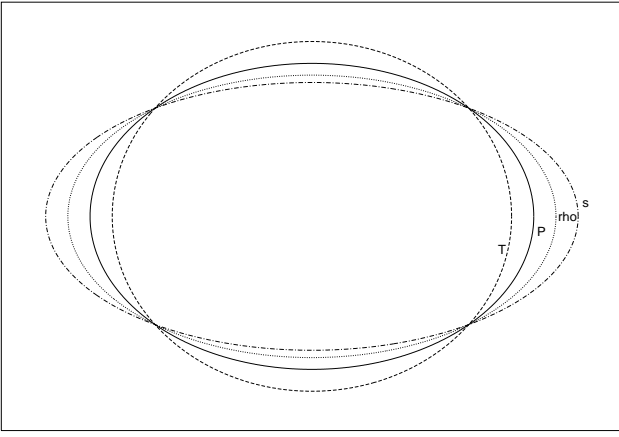


Fig. 27. Surfaces of constant pressure (solid line), constant temperature (dashed line), constant entropy (dash-dotted line), and constant density (dotted line) in a radiative region of a rotating star.

5. Towards an understanding of the internal mass motions

5.1. Internal mass motions in the common envelope

So far Roche geometry has been assumed and the effects of internal mass motions on the equation of hydrostatic equilibrium have been neglected. This is justified as a close approximation to real systems, but a closer look into the layers in the common envelope reveals an inconsistency. This inconsistency can be removed by a slight modification, and this procedure offers insight into the internal mass motions in the common envelope.

As noted in Sect. 2.5, in the present approximate treatment the pressure difference ΔP on equipotential surfaces is negative apart from the surface. For the layers in the common envelope of system 2 this is shown by the strong lines in Fig. 26. Since the large-scale mass motions are driven by pressure differences on equipotential surfaces, and since this difference is negative in each layer, mass is flowing from the secondary to the primary but not from the primary to the secondary. This is incompatible with a configuration in thermal equilibrium with a vanishing net rate of mass transfer.

Can this inconsistency be removed by a slight modification of the structure equations, taking into account internal mass motions? The pressure difference in the common envelope is largest (apart from the sign) in the layers just above the critical surface, causing a mass flow from the secondary to the primary in these layers. In a slightly changed and more consistent treatment this feature is preserved. We need therefore a flow from the primary to the secondary in the outermost layers in order to obtain a vanishing net rate. The resulting velocity field is of the type discussed by Nariai (1976) and Zhou & Leung (1990).

The effects of this velocity field on the run of pressure in the common envelope are determined by a modified surface condition (the generalization of the Roche equipotential condition), a change of the effective gravity, and (since the motions are expected to be turbulent) the presence of a turbulent pressure. We shall discuss these effects in turn. Note that the Roche

potential is well defined and that the difference between Roche potential and effective potential is negligible in the common envelope. The pressure can therefore be treated as a function of the potential. Since we ask for slight changes, we may assume that the change of a curve in Fig. 26 is a superposition of a horizontal shift (caused by the change in the surface condition) and a change in the pressure gradient (caused by the change in the effective gravity and by the turbulent pressure). To reduce the inconsistency we need a shift to the left/right or a decrease/increase in the gradient of the secondary's/primary's curve.

Since the velocity field has a reversing layer, from Bernoulli's equation the surface condition

$$\Psi_1 + \frac{\langle v_1^2 \rangle}{2} = \Psi_2 + \frac{\langle v_2^2 \rangle}{2} \quad (13)$$

is obtained, where v_i is the velocity at the surface of the component i and the angle brackets denote a spherical average, cf. Kähler (1995). Since the pressure vanishes at the surfaces, the surface condition acts as a boundary condition for the run of pressure. Assuming a horizontal shift of the curves, it can be verified that a reduction of the inconsistency requires that

$$\langle v_2^2 \rangle > \langle v_1^2 \rangle, \quad (14)$$

i.e. that the velocities in the secondary are larger than in the primary. The dotted line in Fig. 26 shows an example for the result of a horizontal shift of the secondary's curve. It is manifest that the inconsistency can be removed in this way.

Consider next the effective gravity. In the presence of internal mass motions g_i has to be replaced by

$$\tilde{g}_i = \frac{Gm_i}{r_i^2} - \frac{2}{3}\Omega_i^2 r_i, \quad \text{with } \Omega_i^2 > \omega^2, \quad (15)$$

i.e. the effective gravity is reduced (Kähler 1995). This implies that also the pressure gradient is reduced. If this occurs in the secondary, again the inconsistency is reduced since the pressure at the critical surface decreases.

It remains to discuss the turbulent pressure. Let $P_{g,i}$ be the gas pressure and $P_i = f_i P_{g,i}$ the total pressure. Neglecting the radiation pressure we have $f_i = 1$ in the absence of internal mass motions and $f_i \simeq 2$ if the turbulent velocities are comparable with the sound velocity. Combining the equation of hydrostatic equilibrium and the equation of state we find

$$\frac{d}{dr_i} \ln P_i = -\frac{\mu_i}{\mathfrak{R}T_i} \frac{\tilde{g}_i}{f_i}. \quad (16)$$

Accordingly, an increase in f_i has the same effect as a decrease in the effective gravity. Turbulent pressure reduces the pressure gradient. If this occurs mainly in the secondary, the inconsistency is again reduced.

The discussion of the three effects has shown that the inconsistency can be removed by mass motions which are larger in the secondary than in the primary. Pressure differences in the layers above the critical surface provide the driving mechanism for the velocity field in the common envelope. The result is a field with a reversing layer, with motions from the secondary to the primary in the region above the critical surface and from

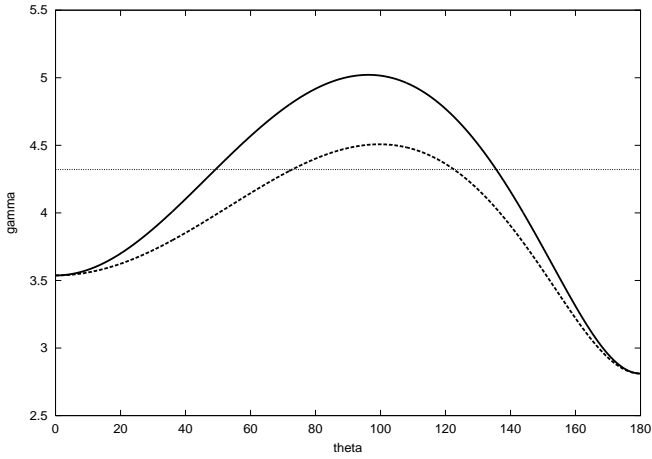


Fig. 28. The normalized gravity γ at the top of the radiative interior in the secondary of AB And, in dependence of the angular distance (in degrees) ϑ from the x -axis. Shown is the run of γ in the plane containing the rotation axis (solid line) and in the equatorial plane (dashed line). The dotted line shows the averaged gravity.

the primary to the secondary in the surface layers, and with velocities which are larger in the secondary than in the primary. Martin & Davey (1995) obtained in hydrodynamic simulations a velocity field with the same properties.

The arguments presented in this subsection concern late-type as well as early-type systems. They are not conclusive since in a spherically averaged treatment of the components degrees of freedom of the internal mass motions escape notice.

5.2. Circulation currents in single stars

Consider first the radiative envelope of an early-type single star in almost uniform rotation. Near the boundary to the convective core as well as near the surface viscous effects are important as discussed by Tassoul & Tassoul (1995), but in the bulk of the envelope the original inviscid solution of Sweet (1950) is a reasonable approximation. Accordingly, on an isobaric surface the temperature is higher around the poles (where the gravity is larger) than around the equator (where the gravity is smaller). The resulting topology of the surfaces of constant thermodynamic quantities is shown in Fig. 27. The eccentricity is smallest in the surface of constant temperature and largest in the surface of constant entropy. We shall need the result that also on a surface of constant entropy the temperature is larger around the poles than around the equator.

Let $l(s)$ be the luminosity carried through the surface $s = \text{const}$, which is the sum

$$l(s) = l_{\text{rad}}(s) + l_{\text{circ}}(s) \quad (17)$$

of the radiative luminosity l_{rad} and the circulation luminosity l_{circ} . In thermal equilibrium and outside the core with nuclear burning we have $dl/ds = 0$ and thus

$$dl_{\text{circ}}/ds = -dl_{\text{rad}}/ds. \quad (18)$$

Assuming stationary currents the heat equation reduces to

$$\text{div} \mathbf{F} = -\rho T \mathbf{u} \cdot \text{grad} s, \quad (19)$$

where \mathbf{F} denotes the radiative flux and \mathbf{u} is the circulation velocity. We integrate this equation over the volume enclosed by the surfaces $s = s_1$ and $s = s_2$, where the difference $s_2 - s_1$ is positive and infinitesimal. The result is

$$l_{\text{rad}}(s_2) - l_{\text{rad}}(s_1) = -(s_2 - s_1) \int_{s=s_1}^{s=s_2} \rho T (\mathbf{u} \cdot \mathbf{n}) dA, \quad (20)$$

where $\mathbf{n} = \text{grad} s / |\text{grad} s|$ is the outward directed normal on the surface $s = s_2$ and dA is an element of this surface. Let \bar{T} be the average of T on this surface and $\Delta T = T - \bar{T}$. Since the net mass flow through the surface vanishes we obtain

$$\frac{dl_{\text{rad}}}{ds} = - \int \Delta T \rho (\mathbf{u} \cdot \mathbf{n}) dA. \quad (21)$$

Since ΔT and $\mathbf{u} \cdot \mathbf{n}$ have the same sign almost everywhere, positive around the pole and negative around the equator, the integrand is positive almost everywhere. Therefore dl_{rad}/ds is negative, and from Eq. (18) we see that dl_{circ}/ds is positive. A slightly generalized discussion shows that this result remains valid in the presence of nuclear burning.

We conclude that radiative layers are sources of the circulation luminosity. The circulation luminosity is positive and a monotonically increasing function of s or of the mass variable. These results concern the bulk of the radiative envelope where viscosity is unimportant, but not the regions at the borders of the envelope. Recall that sinks near the surface are needed.

5.3. Circulation currents in contact binaries

First let us ask for the changes of the gravity g on a level surface in the secondary's interior. The mass m_2 enclosed by this surface is known from the spherically averaged treatment of the system. In a close approximation g is (apart from the sign) the gradient of the potential

$$- \frac{GM_1}{d_1} - \frac{Gm_2}{d_2} - \frac{1}{2} \omega^2 d^2, \quad (22)$$

where d_i is the distance from the centre of the component i and d is the distance from the rotation axis.

Taking the secondary of AB And as an example, Fig. 28 shows the normalized gravity $\gamma = gA^2/(GM)$ at the bottom of the convective envelope, i.e. at the top of the radiative interior. The dashed line shows γ in the equatorial plane in dependence on the angular distance ϑ from the x -axis. (As usual, the x -axis is taken to lie along the line of centres of the components, with the origin in the primary's centre.) The solid line shows the run of γ in the plane containing the rotation axis, and the dotted line denotes the averaged gravity obtained in a spherical treatment of the components. The curves show that the gravity changes almost by a factor of two. On level surfaces deep in the interior the variation is smaller, but on the surface having (in a spherical treatment) the fractional radius 0.5 the gravity still changes by about 10 percent.

On each level surface the gravity is largest at the poles (solid curve for $\vartheta = 90^\circ$), small near $\vartheta = 0^\circ$, and smallest

when $\vartheta = 180^\circ$, i.e. when closest to the inner Lagrangian point. On account of tidal synchronization the rotation is known to be almost uniform. Although the departures from sphericity in the outer layers are large and although the geometry is more complex than in single stars, the essential features are similar. We therefore expect rising motions at the poles and sinking motions at the equator, at least near the x -axis. Similar motions are expected also in the primary.

This is supported by results on radiative regions in uniform rotation (Mestel 1966). They predict a double-cell pattern with a circulation inversion on the level surface with the density $\rho = \omega^2/(2\pi G)$. In AB And the outer cell is absent in the primary (since the critical density occurs in the convective envelope) and unimportant in the secondary since the bulk of the radiative interior is covered by the inner cell. In this cell the circulation is upward/downward in regions of higher/lower gravity. Mestel's result concerns an idealized problem since barotropy is assumed and viscosity is neglected. Questions about the validity of Mestel's result (Tassoul & Tassoul 1995) concern the outer cell and the region around the circulation inversion, but not the bulk of the radiative region where Sweet's (1950) results are confirmed.

Accordingly, it is certain that on an isobaric surface the density is lower in regions of outward motions than in regions of inward motions. Therefore the discussion of the preceding subsection applies, showing that there are sources of the circulation luminosity throughout the bulk of the radiative interior. This is in line with the basic assumption made in Sect. 1. It is also in line with the result from Sect. 2.2 that stable systems have sources not only in the outer layers but also deep in the interior. The corresponding sinks occur either in the outermost radiative layers or in the common turbulent envelope.

6. Summarizing and concluding remarks

The present investigation was based on the assumption that the circulation luminosity in the secondary's interior is positive and large enough to enable thermal equilibrium. The first part of this assumption can be abandoned. As shown in the preceding section the circulation luminosity is certainly positive in the radiative interior, not only in the secondary but also in the primary. In systems with intermediate or small mass ratios the effects in the primary are small while the effects in the secondary are important since the core luminosity is small. In systems with large mass ratios (e.g. OO Aql) the neglect of the circulation luminosity in the primary introduces a slight error.

The resulting treatment of contact binaries is simple. Sources of the circulation luminosity deep in the secondary's interior are necessary, but details are unimportant. Free parameters are the temperature difference between the components ΔT_e , bound to be positive and small, and the efficiency f_E of the energy transfer between the components. The fractional extent of radiative regions is larger in the secondary than in the primary. In the course of evolution the period increases and the mass ratio decreases.

Adopting standard values for the parameters, a survey of unevolved and evolved contact configuration has been obtained. The results are successful in explaining the basic ob-

servational facts, in particular the preference for shallow contact, the minimum period and the minimum temperature, the existence of stable configurations with mass ratios very close to unity, and the period-colour relation. Since stability considerations are essential in these observational tests we consider the results as strong arguments not only in favour of thermal equilibrium but also in favour of the treatment of the stability problem.

Assuming thermal equilibrium, models of individual observed systems with reliable data are well-determined apart from some freedom in ΔT_e . When stable they can be used to calibrate the efficiency and to determine metallicity and age. The models obtained so far are stable, which lends again support to the assumption of thermal equilibrium. Evolutionary effects are important. The efficiency is very small ($f_E = 10^{-3} \dots 10^{-5}$).

Concerning the hydrodynamic problem, arguments have been presented that the velocity field in the common envelope has a reversing layer with motions from the secondary to the primary in the layers just above the critical surface and from the primary to the secondary in the surface layers.

Details of the circulation, in particular the circulation function, can be determined only in a three-dimensional discussion. In comparison with rotating stars the problem is more difficult since the geometry is more complex. In other respects the problem is simpler since rotation law and geometry are known in a close approximation. This problem will be investigated in a forthcoming paper, again assuming thermal equilibrium.

Although we have strong arguments in favour of thermal equilibrium we have no proof, and it is uncertain whether a proof is possible.

References

- Eggen O. J. 1961, R. Greenwich Obs. Bull. 31
- Eggen O. J. 1967, Mem. R. Astron. Soc. 70, 111
- Hazlehurst J. 1974, A&A 36, 49
- Hazlehurst J. 1993, A&A 271, 209
- Hilditch R. W., King D. J., & McFarlane T. M. 1988, MNRAS 231, 341
- Hrivnak B. J. 1988, ApJ 335, 319
- Hrivnak B. J. 1989, ApJ 340, 458
- Kähler H. 1986, A&A 157, 329
- Kähler H. 1989, A&A 209, 67
- Kähler H. 1995, A&A 294, 497
- Kähler H. 2002, A&A 395, 899
- Kähler H. 2002, A&A 395, 907
- Kähler H., & Fehlberg H.-J. 1991, A&A 252, 137
- Kaluzny J., Rucinski S. M. 1986, AJ 92, 666
- Kippenhahn R. 1963, ApJ 137, 664
- Lucy L. B. 1968, ApJ 151, 1123
- Maeder A., & Zahn J.-P. 1998, A&A 334, 1000
- Martin T. J., & Davey S. C. 1995, MNRAS 275, 31
- Mestel L. 1965, in Stars and Stellar Systems, Vol. VIII (The University of Chicago Press, Chicago, London)
- Mestel L. 1966, ZAp 63, 196
- Mochnecki S.W. 1984, ApJS 55, 551
- Moss D. L., & Whelan J. A. J. 1973, MNRAS 161, 239
- Nariai K. 1976, PASJ 28, 587
- Roxburgh I. W., Griffith J. S., & Sweet P. A. 1965, ZAp 61, 203

- Ruciński S. M. 1993, in *The realm of interacting binary stars*, ed. J. Sahade, G. E. Mc Cluskey, & Y. Kondo (Kluwer, Dordrecht)
- Sweet P. A. 1950, *MNRAS* 110, 548
- Rucinski S.M., Lu W., & Mochnacki S.W. 2000, *AJ* 120, 1133
- Tassoul M., & Tassoul J. L. 1995, *ApJ* 440, 789
- Zhou D. Q., & Leung K. C. 1990, *ApJ* 355, 271